

# Method for Detection of Nuclear-Plasma Interactions in a $^{134}\text{Xe}$ -Doped Exploding Pusher at the National Ignition Facility<sup>\*)</sup>

Darren L. BLEUEL<sup>1)</sup>, Lee A. BERNSTEIN<sup>1)</sup>, Christopher A. BRAND<sup>1,2)</sup>, William S. CASSATA<sup>1)</sup>, Brian H. DAUB<sup>1,2)</sup>, Lucile S. DAUFFY<sup>1)</sup>, Bethany L. GOLDBLUM<sup>2)</sup>, James M. HALL<sup>1)</sup>, Chris A. HAGMANN<sup>1)</sup>, Laura Berzak HOPKINS<sup>1)</sup>, Hesham Y. KHATER<sup>1)</sup>, Andrea L. KRITCHER<sup>1)</sup>, Dieter H. G. SCHNEIDER<sup>1)</sup>, Sunniva SIEM<sup>3)</sup>, Carol A. VELSKO<sup>1)</sup> and Mathis WIEDEKING<sup>4)</sup>

<sup>1)</sup>Lawrence Livermore National Laboratory, Livermore, CA 94550, USA

<sup>2)</sup>University of California, Berkeley, CA 94720, USA

<sup>3)</sup>University of Oslo, N-0316 Oslo, Norway

<sup>4)</sup>iThemba LABS, Somerset West 7129, South Africa

(Received 10 July 2015 / Accepted 26 February 2016)

Angular momentum changes due to nuclear-plasma interactions on highly-excited nuclei in high energy density plasmas created at the National Ignition Facility can be measured through a change in isomer feeding following gamma emission. We propose an experiment to detect these effects in  $^{133}\text{Xe}^*$  in exploding pusher capsules.

© 2016 The Japan Society of Plasma Science and Nuclear Fusion Research

Keywords: nuclear, plasma, laser, isomer, high energy density, activation, fusion

DOI: 10.1585/pfr.11.3401075

## 1. Introduction

Electron-mediated nuclear-plasma interactions (NPIs) such as Nuclear Excitation by Electron Capture (NEEC) or Transition (NEET) are expected to cause significant changes in reaction cross sections in High Energy Density Plasmas (HEDPs) such as nuclear weapons tests, National Ignition Facility (NIF) shots, and astrophysical settings. However, NPIs remain largely unobserved due to the extreme narrowness of nuclear transitions ( $\Gamma \leq 1 \mu\text{eV}$ ). A schematic of the NEEC and NEET processes are shown in Fig. 1. In both cases, the atomic binding energies are modified in the plasma environment due to charge state and screening effects. For NEEC, an electron is resonantly captured into an atomic orbital where the binding energy plus the electron kinetic energy is equal to the first excited nuclear state (for excitations off the ground state). For the NEET process, atomic electrons transition with a binding energy difference equal to the nuclear excitation energy. Then, the binding energy (for NEET) or the free electron energy plus the binding energy (for NEEC) is resonantly transferred to the nucleus via a virtual photon and the nucleus becomes excited.

HEDP environments are expected to have a significant effect on cosmogenic nucleosynthesis, the formation of heavy elements from pre-existing nucleons in astrophysical plasmas [1]. Nuclei in stellar plasmas reach a thermal population of low-lying excited nuclear states from photo-

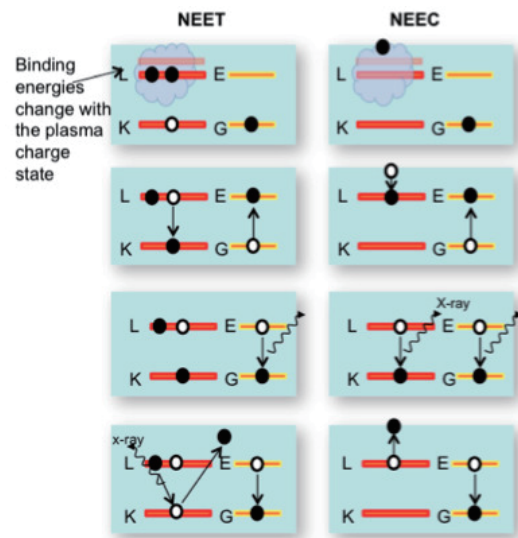


Fig. 1 Schematic of the NEET (left) and NEEC (right) processes. The red levels denote the atomic shells (L and M) and the yellow levels denote the nuclear excited and ground states (E and G). The top two boxes depict the excitation method while the bottom two show two different de-excitation schemes.

excitation, NEEC, NEET, and inelastic electron scattering in the dense plasma. Thermally-excited nuclei have different spin, parity, and Q values leading to significantly modified neutron capture cross sections, and therefore different isotopic and elemental abundances. The ratio of capture cross sections for thermally-excited nuclei com-

author's e-mail: bleuel1@llnl.gov

<sup>\*)</sup> This article is based on the presentation at the Conference on Laser Energetics 2015 (CLE2015).

pared to ground state nuclei is referred to as the stellar enhancement factor (SEF). In addition to this well-known but experimentally-unobserved effect of NPIs on low-lying nuclear states, NPIs may affect thermal neutron capture cross sections after the absorption of a neutron but before subsequent emission of a gamma ray. In such a case, small increases in angular momentum near the neutron separation energy due to NPIs dramatically increase the probability of neutron re-emission. The relevance of these processes to post-capture nuclei is subject to a competition between the short lifetimes ( $\sim$ fs) of highly-excited states versus the large number of nuclear transitions available and high electron and photon fluxes. Modeling of these effects is unwieldy due to the large number of both atomic and nuclear transitions possible, necessitating experimental measurements.

Although there have been extensive theoretical studies on this subject, previous attempts to measure NEEC have been unsuccessful [2], including our own attempts [3] to detect the NEEC process by resonantly exciting the ground state of  $^{181}\text{Ta}$  and  $^{187}\text{Os}$  in plasmas generated at the Omega Facility at the Laboratory for Laser Energetics at the University of Rochester. The limited observations of the parallel bound-state process NEET are controversial and have been restricted to non-plasma environments [4–6]. We will overcome this challenge by inducing NPIs on highly-excited ( $\sim 1$ –5 MeV) nuclear states produced by nuclear reactions *prior* to their decay by spontaneous gamma-ray emission. The large density of nuclear states ( $\geq 10^{-1}$ – $10^0$  eV $^{-1}$ ) at these excitation energies increases the probability that the energy from the atomic transition will resonantly match an available nuclear transition. In addition, we will exploit a new experimental signature—the differential population of a high-spin isomer—to observe these effects.

## 2. The Double Isomer-to-Ground State (DIGS) Ratio: a Signature of NPIs

A major challenge in the search for NPIs is the observation of a clear signature of the effect in a highly-chaotic HEDP environment. The energy transfer is usually small (keV) and the subsequently emitted radiation is overwhelmed by the background radiation in the HEDP. We propose a new signature for NPIs on highly-excited nuclei: the differential population of an isomeric state versus the ground state of the de-excited nucleus.

While ( $n, \gamma$ ) reactions are of primary importance to astrophysical and other HEDP environments, we may observe the same NPI effects following ( $n, 2n$ ) reactions at the NIF, which initially populate states several MeV below the neutron separation energy prior to gamma emission. Though energy transfer by NPIs is small, changes in angular momentum can accompany this small energy transfer in highly-excited nuclei following ( $n, 2n$ ) reactions but prior

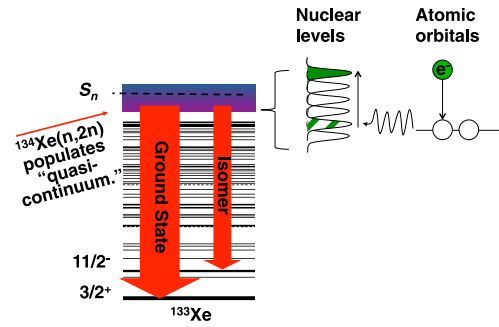


Fig. 2 Electron-mediated nuclear-plasma interactions change the angular momentum distribution, leading to a change in subsequent isomer population.

to gamma emission. An experimentally-accessible candidate is  $^{133}\text{Xe}^*$ , created in  $^{134}\text{Xe}(n, 2n)$  reactions, which has a long-lived 11/2- isomer and a 3/2+ ground state. The capability of NPIs to produce differential isomer population for reactions in versus out of a plasma is shown schematically in Fig. 2. The double isomer-to-ground-state (DIGS) ratio is defined as

$$R_{\text{DIGS}} = \frac{N_{\text{capsule}}^{\text{Xe-133m}} / N_{\text{capsule}}^{\text{Xe-133g}}}{N_{\text{TOAD}}^{\text{Xe-133m}} / N_{\text{TOAD}}^{\text{Xe-133g}}}, \quad (1)$$

where  $N$  is the number of each state populated, determined from its characteristic-energy gamma ray emissions measured in a high-purity germanium detector. A non-unity DIGS ratio for the  $^{133m}\text{Xe}/^{133g}\text{Xe}$  fraction formed in an exploding pusher capsule plasma divided by same quantity for an externally-mounted, non-plasma “TOAD” (Target Option Activation Device) sample will show NPIs took place on highly-excited states in  $^{133}\text{Xe}$ .

## 3. Proposed Experiment

The National Ignition Facility (NIF) uses up to 2 MJ of laser energy to implode capsules of deuterium-tritium fusion fuel to pressures, densities, and temperatures similar to the core of the sun [7]. The combination of the large instantaneous neutron, photon and electron fluxes present in a NIF capsule is a unique environment for probing the interaction between highly-excited nuclear states with a HEDP. We propose an experiment at the NIF to observe NPIs on highly-excited  $^{133}\text{Xe}^*$  using an existing platform and diagnostics. A standard indirect-drive exploding pusher platform [8] will be used, consisting of a gold hohlraum filled with low-density (0.03 mg/cc) helium gas surrounding a thin (120–175  $\mu\text{m}$ ) plastic (CH with a graded silicon dopant) shell/capsule filled with 10 atm DT gas. Because of the low compression and low capsule shell areal density, the exploding pusher platform, originally designed for diagnostic calibration, has also been used for controlled experiments [9] requiring evenly-heated and evenly-compressed plasmas and an unattenuated, isotropic, 14 MeV neutron source. The capsule gas

will be doped with 0.03 atm isotopically-pure (>99%)  $^{134}\text{Xe}$ . Indirect laser drive using 933 kJ of laser energy at a peak power of 325 TW will produce  $>10^{14}$  DT fusion neutrons, inducing  $^{134}\text{Xe}(n, 2n)$  reactions in a  $kT > 5$  keV plasma to produce  $^{133}\text{Xe}^*$  in a highly-excited state a few MeV below the neutron separation energy.

Repeated NPIs in the high energy density plasma will transfer energy and angular momentum, altering the subsequent isomer population. The xenon originally loaded in the capsule will be collected in the existing RAGS (Radiochemical Analysis of Gas Samples) collectors, with measured collection efficiency greater than 50%, and transported to a low-background counting facility. As a control,  $^{134}\text{Xe}$  will also be loaded into one or more “TOAD” sealed containers located 50 cm from the implosion on up to three Diagnostic Instrument Manipulators (DIMs) irradiated with the same neutron spectrum. The thin shell and low compression of the exploding pusher ensures minimal difference between the original fusion neutron spectrum (overwhelmingly 14 MeV) in the plasma and that incident on the TOADs. The post-shot TOAD samples will be retrieved and also taken to a low-background facility for counting on the same detectors such that systematic uncertainties are the same between each sample and cancel in the DIGS ratio. The  $^{133m}\text{Xe}$  isomer emits a 233 keV gamma ray with a half life of 2.19 days while the  $^{133g}\text{Xe}$  ground state beta decays, emitting an 81 keV gamma ray with a 5.43 day half life. Thus sufficient time is available for sample retrieval and delivery without significant decay of the species to be measured.

A previous NIF direct-drive exploding pusher shot (N120228-001) with 0.057 atms of a 52/44/4 mix of  $^{124}\text{Xe}$ ,  $^{126}\text{Xe}$  and  $^{128}\text{Xe}$  doping demonstrated the feasibility of irradiating, collecting, and counting xenon activation products [10]. The radioactive  $^{123,125,127}\text{Xe}$  products were collected using RAGS and counted  $\approx 5$  hours after the shot at the Building 151 nuclear counting facility at Lawrence Livermore National Laboratory.

The measured relative  $^{126}\text{Xe}(n, 2n)/^{124}\text{Xe}(n, 2n)$  ratio was  $1.22 \pm 0.05$  ( $\sigma_{\text{statistical}} = 4.1\%$ ). We anticipate better counting statistics in our experiment since the  $^{133m}\text{Xe}$  and  $^{133g}\text{Xe}$  are significantly longer-lived than the  $^{123,125}\text{Xe}$  radionuclides (2.00 and 17.1 hr respectively) resulting in fewer lost decays during retrieval and transport. Furthermore, the samples will be counted much closer to the detector (since only the ratio of the gamma-ray intensities and not their absolute magnitudes are important), and the yield will be higher. A statistical uncertainty of less than 1% is easily achievable based on these improvements.

The TOAD has an interior gas volume of  $34.3 \text{ cm}^3$ . For a NIF shot yield of  $10^{14}$  neutrons, the fluence at 50 cm from the implosion where the TOAD is located will be  $3 \times 10^9 \text{ n/cm}^2$ , inducing  $6 \times 10^6 (n, 2n)$  reactions. This is more than sufficient to detect more than 10,000  $\gamma$  rays, achieving  $< 1\%$  statistical uncertainty, in a high-purity germanium detector with  $\sim 1\%$  photopeak efficiency over a several-day

measurement.

A potential background source of non-plasma xenon reaction products collected by RAGS is due to neutrons reacting with residual xenon in the capsule fill tube. An MCNP [11] simulation, conservatively assuming no attenuation, constant temperature and pressure, and a capsule compression to 200  $\mu\text{m}$  (similar to the NIF shot designated N130503), has shown this contributes no more than  $10^{-5}$  the number of reactions as in the capsule.

Another potential background source of  $^{134}\text{Xe}$  production is from thermal neutrons, which may induce  $^{132}\text{Xe}(n, \gamma)^{133}\text{Xe}$  reactions on small impurities in the xenon gas. With an expected 0.3%  $^{132}\text{Xe}$  impurity in a 99% enriched  $^{134}\text{Xe}$  gas and a thermal neutron fraction of 3% of the 14 MeV fluence, the fraction of  $^{133}\text{Xe}$  produced from these  $(n, \gamma)$  reactions only is  $2.5 \times 10^{-5}$ .

While the thermal cross section for  $^{133}\text{Xe}(n, \gamma)^{134}\text{Xe}$  is quite high (190 b), no significant depletion of the  $^{133}\text{Xe}$  product is expected due to the low number density of nuclei produced ( $\sim 10^{-12}$  of the  $^{132}\text{Xe}$  impurity).

The Hauser-Feshbach nuclear reactions code, TALYS [12] was used to predict isomer and ground state population from this reaction. By default, TALYS uses the first ten known discrete levels in  $^{133}\text{Xe}$ , above which a level density model is used. This number was increased to 28 to include known, prominent, low-lying, isomer-feeding states (such as the twelfth level at 1.1695 MeV with  $J = 13/2^-$ ). Changing this parameter, TALYS predicts cross sections of the  $^{134}\text{Xe}(n, 2n)$  reaction leading to the isomer and ground state of  $^{133}\text{Xe}$  to be, respectively, 0.75 b and 0.93 b, consistent with the limited experimental data available for this reaction [13, 14]. Thus these TALYS level parameters were later used (see next Section) to predict the cross sections at lower energies where measurements are unavailable. The ratio of this isomer cross section to the ground state cross section is 0.8. This near-equal population of each state provides ideal detection statistics and sensitivity to perturbation.

The baseline population  $^{133m}\text{Xe}/^{133g}\text{Xe}$  ratio from 14 MeV neutrons was measured using the DT generator located at iThemba LABS in South Africa. Results from that experiment are currently under analysis. Further quantification of background reactions and rate parameters could be obtained through thermal neutron capture experiments on  $^{132}\text{Xe}$  at a reactor or other thermal neutron source, and radiative strength function/level density measurements using the “Oslo method” [15] in inverse kinematics at iThemba using the  $d(^{132}\text{Xe}, ^{133}\text{Xe}^*)p$  reaction.

#### 4. MCNP Modeling of the Neutron Scatter Effect on the DIGS Ratio

A significant uncertainty in Eq. 1 can arise from neutrons scattering off DIMs and other chamber components such that the neutron spectra in and out of the plasma (capsule vs. TOAD) may not be precisely identical. This ef-

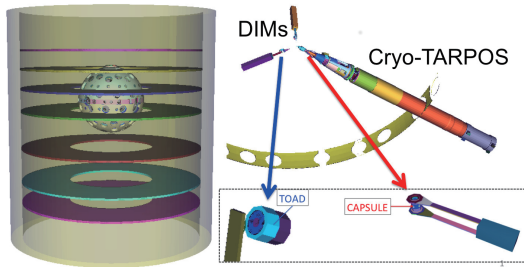


Fig. 3 Geometry of NIF chamber and internal components modeled with MCNP to determine neutron downscatter in the TOAD xenon. The NIF chamber and target bay (left) surround the DIMs and cryo-TARPOS (right). Each DIM holds a TOAD (bottom left) and the capsule is contained within a hohlraum in the thermomechanical package (bottom right) at the end of the cryo-TARPOS.

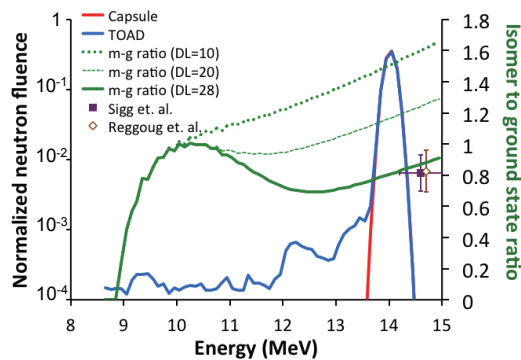


Fig. 4 Normalized neutron spectra ( $n/cm^2/MeV$  which integrates to unity over all energies) in the capsule (red) and the TOAD (blue) above the 8.6 MeV threshold, along with the isomer-to-ground state (m-g) cross section ratio (green, right axis) produced in  $^{134}\text{Xe}(n, 2n)$  reactions predicted by TALYS for both the default number of discrete levels used ( $DL = 10$ ) and increased values ( $DL = 20$  and  $28$ ). Experimentally-measured ratios [13, 14] are noted by datapoints. Statistical uncertainties in the neutron spectra are smaller than the datapoints.

fect has been quantified with MCNP modeling of the NIF chamber and target bay, including the capsule, thermo-mechanical package, cryo-TARPOS, three DIMs, and a TOAD mounted to the side of each DIM, elements of which are depicted in Fig. 3. From the energy-dependent isomer-to-ground state ratio calculated with TALYS (see previous Section) shown in Fig. 4, it is apparent that neutrons scattering off components in the NIF chamber to lower energies (down to the  $(n, 2n)$  threshold of 8.6 MeV) will decrease the isomer-to-ground state population in the TOAD, increasing the DIGS ratio defined in Eq. 1. If uncorrected, this will mask NPI effects expected to decrease the DIGS ratio.

The neutron flux inside the imploding capsule and inside the  $^{134}\text{Xe}$  gas contained in the 1 mm thick aluminum TOAD are also shown in Fig. 4. Convoluting these spectra with the calculated cross sections including all 28 known

discrete levels in the model, it is predicted that the difference in neutron spectra will produce only a 0.12% increase in the DIGS ratio, independent of NPI effects.

The small magnitude of this effect can be attributed to both the low amount of neutron scatter into the 8 - 14 MeV region and the relative invariance of the isomer-to-ground state ratio as a function of neutron energy. In a more conservative assumption, if the number of discrete levels included in TALYS is reduced to 20, the effect of the scattered neutrons on the DIGS ratio is still only 0.21%. Major sources of scattered neutrons in this latter, more conservative, simulation include the hohlraum (increasing DIGS 0.02%), the tantalum blast plate in front of the TOAD (0.02%) the aluminum TOAD walls (0.05%), the aluminum mount behind the TOAD (0.03%), the DIM (0.05%), and the xenon gas itself (0.03%).

Replacing all the aluminum components of the TOAD and mount with a high-Z material like tantalum reduces this effect by about half. Such a redesign would improve the measurement, but is deemed unnecessary given the small and calculable effect.

The deployment of multiple TOADs of varying materials and thicknesses on up to three DIMs with different lines-of-sight in test shots will provide confidence in this modeling. Any changes in the DIGS ratio from one position to another, will indicate scattering effects rather than NPis.

## 5. Predicted Results

Predicting the exact impact of NPis on the relative populations of  $^{133m}\text{Xe}$  and  $^{133g}\text{Xe}$  is a significant challenge, due in part to the extremely large number of possible atomic transitions coupled to a similarly large number of nuclear transitions. The probability of an NPI is also extremely uncertain due to its dependence on the low-energy (keV) photon transition strength, characteristic of the Xe M-, L-, and K-shell atomic binding energies.

Top to bottom, respectively, Fig. 5 shows the initial excitation energy and angular momentum states populated immediately after  $^{134}\text{Xe}(n, 2n)^{133g}\text{Xe}^*$ , the subsequent gamma decay path predicted (in the absence of NPis), and the angular momentum distribution of the nucleus' actual levels predicted by TALYS. Multiple NPis will on average shift the angular momentum towards the actual available level distribution, overall lowering the angular momentum distribution as the nucleus decays by gamma-ray emission as indicated in the lower panel of Fig. 5. This lowering of angular momentum will increase the proportion of decays that populate the lower-spin ground state of  $^{133g}\text{Xe}$  versus the higher-spin  $^{133m}\text{Xe}$  isomer.

In order to determine the impact of NPis on isomer population, we must consider both the transition rate of the NPis, and how this additional decay channel will modify normal nuclear decay.

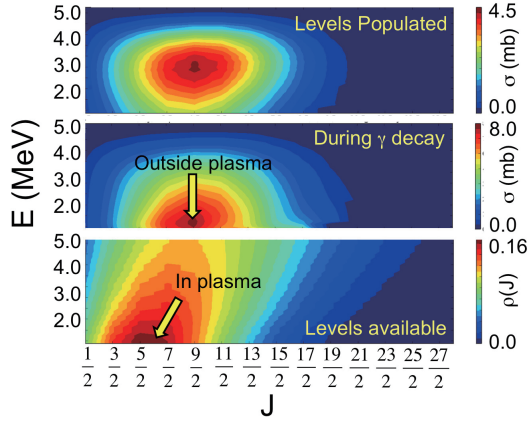


Fig. 5 TALYS predictions of the energy ( $E$ ) and angular distribution ( $J$ ) of states populated immediately following  $^{134}\text{Xe}(n, 2n)^{133}\text{Xe}^*$  reactions (top), the predicted unperturbed gamma decay path (middle), versus the  $E/J$  distribution of actual available states (bottom).

### 5.1 NPI rate

To determine the rate of NPIs on an excited state, we assume a local thermal equilibrium environment and use the principle of detailed balance, following the methodology of Gosselin and Morel [16] in which the rate of NEEC between an initial state  $i$  and a final state  $f$  is given by

$$\lambda_d^{NEEC} = \frac{2J_f + 1}{2J_i + 1} \frac{\alpha(T_e) \ln(2)}{T_{i \rightarrow f}^\gamma} f_{FD}(E_b)(1 - f_{FD}(E_r)) \times \frac{1}{2} \left( \operatorname{erf}\left(\frac{E_r}{\varepsilon \sqrt{2}}\right) - \operatorname{erf}\left(\frac{E_b}{\varepsilon \sqrt{2}}\right) \right), \quad (2)$$

where  $J_i$  and  $J_f$  are the spins of states  $i$  and  $f$ ;  $\alpha(T_e)$  is the internal conversion coefficient for the  $i \rightarrow f$  transition;  $T_{i \rightarrow f}^\gamma$  is the radiative lifetime of the transition;  $f_{FD}$  is the Fermi-Dirac function;  $E_r$  and  $E_b$  are the free and bound electron energies, which are assumed to resonantly match the  $i \rightarrow f$  transition, and  $\varepsilon$  is the dispersion of the electronic transition energy around the average atom value.

Rather than using the average atom model, however, we use the calculated energies of specific states and configurations from the atomic physics code FLYCHK [17], which replaces the error functions with a sum over all bound states  $b$ . Furthermore, we assume that our initial state  $i$  is in the quasi-continuum, and so instead of a single state  $f$ , we consider all possible final nuclear states, which we represent with the level density  $\rho(E_i + (E_r + |E_b|), J_f)$ , and replace  $T_{i \rightarrow f}^\gamma$  with the average transition strength,

$$\lambda_d^{NEEC} = \sum_{all\ b} \frac{2J_f + 1}{2J_i + 1} \frac{\alpha(T_e) \ln(2)}{\langle T_{i \rightarrow f}^\gamma \rangle} \rho(E_i + (E_r + |E_b|), J_f) \times f_{FD}(E_b)(1 - f_{FD}(E_r)). \quad (3)$$

Now we substitute the expression for the photon strength function,  $S(E_\gamma)$ ,

$$S(E_\gamma) = \frac{\hbar \rho(E_i + E_\gamma, J_f)}{2 \langle T_{i \rightarrow f}^\gamma \rangle E_\gamma^3}, \quad (4)$$

where  $E_\gamma = E_r + |E_b|$ , and finally, we integrate over all possible electron energies with a differential electron flux  $\frac{d\Phi(E_r)}{dE_r}$ , yielding

$$\lambda_d^{NEEC} = \int dE_r \frac{d\Phi(E_r)}{dE_r} \sum_{all\ b} \frac{2J_f + 1}{2J_i + 1} \frac{\alpha(T_e) \ln(2) E_\gamma^3}{\hbar} \times S(E_\gamma) f_{FD}(E_b)(1 - f_{FD}(E_r)). \quad (5)$$

Unfortunately, no measurements of the photon strength function,  $S(E_\gamma)$ , in the quasi-continuum have been made below  $\sim 1$  MeV, which is well above the transition energies where  $\alpha(T_e)$  is substantial. To bound the possible NEEC rate, we consider two possible photon strength functions. The lower bound is based on the assumption that the photon strength function at low energies follows the generalized Lorentzian form seen at higher energies. With this photon strength function and a typical level density in the quasi-continuum, even in very hot, dense plasmas, the NEEC rate is on the order of 1/ns. To determine the upper bound, we assume that the photon strength function is given by the single-particle estimate, in which case the NEEC rate can be as high as  $0.1 - 10 \text{ fs}^{-1}$ .

### 5.2 Gamma-decay modification due to NPIs

To estimate the impact on high spin isomer production, we must include NPIs in a Hauser-Feshbach model. For some initial excited state  $i$ , the total decay width is the sum of all possible partial decay widths. The branching ratio to a specific final state  $f$  is given by the ratio of the partial decay width to this total decay width.

To include the effects of NPIs, we assume a total NPI rate and convert it to a decay width to include among the existing decay channels. We use the reaction code TALYS to perform the standard Hauser-Feshbach calculation, and include the effects of NPIs manually. The initial population in  $E, J$  space for  $^{133}\text{Xe}$  following the  $^{134}\text{Xe}(n, 2n)$  reaction is calculated using TALYS, as well as the total decay width for normal reactions for each  $E, J$  bin. We then sequentially calculate the decay from the highest energy bin. For the assumed NPI rate, the NPI branching ratio for each state is calculated, and this ratio is applied to the population of the state to determine the population which undergoes NPIs. The remaining population is allowed to decay by a single gamma ray, and the new population is added to the initial  $E, J$  population matrix. Because the atomic transition energies are small compared to the typical bin size in the calculation, it is assumed that NPIs do not change the energy bin, and only change the spin. The spin change is allowed to be  $-1, 0$ , or  $+1$ , with a rate proportional to the final state level density for each spin. This results in a new population in the maximum energy bin with a new spin distribution. The process is then repeated, with the proper fraction of the new population being allowed to undergo NPIs, while the rest are allowed to decay normally,

until the population of the highest energy bin falls below  $10^{-8}$  mb/MeV. The process is then begun again with the next highest energy bin. This is repeated until the decay is complete, and then the isomer to ground state ratio is computed. Based on these results, an NPI rate of  $\sim 0.4$  fs $^{-1}$  is required to reduce the isomer to ground state ratio by 5%. A rate of 1/fs will reduce this ratio by 10%. For the lower limit of the NPI rate, based on the generalized Lorentzian photon strength function, no visible impact will be seen in the DIGS ratio, but a 5 - 10% effect will be measurable for the single particle estimate of the PSF.

This analysis neglects the NEET process which may contribute significantly more to the NPI rate. Furthermore, this estimate is also sensitive to the low-energy portion ( $\sim$ keV) of the photon strength function characteristic of the Xenon M-, L-, and K-shell atomic binding energies. The low-energy portion of the strength function in similar-mass nuclei has exhibited an unexpected and unexplained dipole enhancement at low energies [18, 19], deviating dramatically from the Lorentzian models. Only the tail of this enhancement above 1 MeV has been measured, however. Depending on the keV nature of the enhancement, which is not included in the generalized Lorentzian used in TALYS calculations, reaction rates could increase by many orders of magnitude. Even if no change in the DIGS ratio is observed, limits can be set on the low-energy photon transition strength in the quasi-continuum, where no measurements are currently possible and theoretical estimates vary by many orders of magnitude.

## 6. Conclusions

The DIGS ratio is introduced as a signature for detecting angular momentum changes due to NPIs on highly-excited nuclei prior to gamma emission. We propose an experiment at the NIF to detect NPIs using the DIGS ratio in highly-excited  $^{133}\text{Xe}^*$ , produced in  $^{134}\text{Xe}(n, 2n)$  reactions, loaded into an indirect drive exploding pusher capsule. If the DIGS ratio does not deviate from unity, indicating NPI effects, limits can be set on the unknown low-energy photon transition strength in the quasi-continuum. Deviation from unity will indicate, for the first time, the alteration of a nuclear reaction due to a plasma environment.

## Acknowledgements

This work performed under the auspices of the UC Office of the President and the U.S. Department of Energy by Lawrence Livermore National Laboratory under Contract DE-AC52-07NA27344 and the University of California Office of the President Laboratory Fees Research Program under Award 12-LR-238745. Dr. Wiedeking ac-

knowledges support from the National Research Foundation of South Africa.

- [1] Z.Y. Bao, H. Beer, F. Kappeler, F. Voss and K. Wisshak, *Atomic Data Nucl. Data Tables* **76**, 70 (2000).
- [2] Personal Communication with V. Meot, CEA (unpublished).
- [3] A. Kritcher *et al.* (in preparation).
- [4] S. Kishimoto, Y. Yoda, M. Seto, Y. Kobayashi, S. Kitao, R. Haruki, T. Kawauchi, K. Fukutani and T. Okano, *Phys. Rev. Lett.* **85**, 1831 (2000).
- [5] S. Kishimoto, Y. Yoda, Y. Kobayashi, S. Kitao, R. Haruki and M. Seto, *Nucl. Phys. A* **748**, 3 (2005).
- [6] I. Ahmad, R.W. Dunford, H. Esbensen, D.S. Gemmell, E.P. Kanter, U. Rtt and S.H. Southworth, *Phys. Rev. C* **61**, 051304 (2000).
- [7] M.J. Edwards, P.K. Patel, J.D. Lindl, L.J. Atherton, S.H. Glenzer, S.W. Haan, J.D. Kilkenny, O.L. Landen, E.I. Moses *et al.*, *Phys. Plasmas* **20**, 070501 (2013).
- [8] S. Le Pape, L. Divol, L. Berzak Hopkins, A. Mackinnon, N. B. Meezan, D. Casey, J. Frenje, H. Herrmann, J. McNaney *et al.*, *Phys. Rev. Lett.* **112**, 225002 (2014).
- [9] M.J. Rosenberg, A.B. Zylstra, F.H. Sguin, H.G. Rinderknecht, J.A. Frenje, M. Gatu Johnson, H. Sio, C.J. Waugh, N. Sinenian *et al.*, *Phys. Plasmas* **21**, 122712 (2014).
- [10] D.A. Shaughnessy, C.A. Velsko, D.R. Jedlovec, C.B. Yeamans, K.J. Moody, E. Tereshatov, W. Stoeffl and A. Riddle, *Rev. Sci. Instrum.* **83**, 10D917 (2012).
- [11] X-5 MONTE CARLO TEAM, "MCNP - A General Monte Carlo N-Particle Transport Code, Version 5 - Volume I: Overview and Theory", LA-UR-03-1987, Los Alamos National Laboratory, revised 2/2008 (2008).
- [12] A.J. Koning, S. Hilaire and M.C. Duijvestijn, "TALYS-1.0", in *Proceedings of the International Conference on Nuclear Data for Science and Technology*, edited by O. Bersillon, F. Gunsing, E. Bauge, R. Jacqmin and S. Leray (Nice, France, 2007).
- [13] R.A. Sigg and P.K. Kuroda, *Nucl. Sci. Eng.* **60**, 230 (1976).
- [14] A. Reggoug, G. Paic and M. Berrada, "Measurement of (n,2n) reaction cross sections by X-ray spectroscopy", *Prog. Univ. Mohammed V, Rabat, Annual Report No.5*, p.14 (1982).
- [15] A. Schiller, L. Bergholt, M. Guttormsen, E. Melby, J. Rekstad and S. Siem, *Nucl. Instrum. Methods Phys. Res. A* **447**, 498 (2000).
- [16] G. Gosselin and P. Morel, *Phys. Rev. C* **70**, 064603 (2004).
- [17] H.-K. Chung, M.H. Chen, W.L. Morgan, Yu. Ralchenko and R.W. Lee, *High Energy Density Physics* **1**, 3 (2005).
- [18] M. Wiedeking, L.A. Bernstein, M. Krtička, D.L. Bleuel, J.M. Allmond, M.S. Basunia, J.T. Burke, P. Fallon, R.B. Firestone, B.L. Goldblum, R. Hatarik, P.T. Lake, I-Y. Lee, S.R. Leshner, S. Paschalis, M. Petri, L. Phair and N.D. Scielzo, *Phys. Rev. Lett.* **108**, 162503 (2012).
- [19] M. Guttormsen, R. Chankova, U. Agvaanluvsan, E. Algin, L.A. Bernstein, F. Ingebretsen, T. Lönroth, S. Messelt, G. E. Mitchell, J. Rekstad, A. Schiller, S. Siem, A. C. Sunde, A. Voinov and S. Ødegård, *Phys. Rev. C* **71**, 044307 (2005).